

Terahertz-time domain spectrometer with 90 dB peak dynamic range

N. Vieweg · F. Rettich · A. Deninger · H. Roehle ·
R. Dietz · T. Göbel · M. Schell

Received: 24 January 2014 / Accepted: 12 June 2014 /

Published online: 9 July 2014

© The Author(s) 2014. This article is published with open access at Springerlink.com

Abstract Many time-domain terahertz applications require systems with high bandwidth, high signal-to-noise ratio and fast measurement speed. In this paper we present a terahertz time-domain spectrometer based on 1550 nm fiber laser technology and InGaAs photoconductive switches. The delay stage offers both a high scanning speed of up to 60 traces / s and a flexible adjustment of the measurement range from 15 ps – 200 ps. Owing to a precise reconstruction of the time axis, the system achieves a high dynamic range: a single pulse trace of 50 ps is acquired in only 44 ms, and transformed into a spectrum with a peak dynamic range of 60 dB. With 1000 averages, the dynamic range increases to 90 dB and the measurement time still remains well below one minute. We demonstrate the suitability of the system for spectroscopic measurements and terahertz imaging.

Keywords terahertz time domain spectroscopy · femtosecond fiber laser · InGaAs photoconductive switches · terahertz imaging

1 Introduction

Terahertz waves feature unique properties: like microwaves, terahertz radiation passes through a plethora of non-conducting materials, including paper, cardboard, plastics, wood, ceramics and glass-fiber composites [1]. In contrast to microwaves, terahertz waves have a smaller wavelength and thus offer sub-millimeter spatial resolution. Whilst many different techniques coexist today, terahertz generation and detection with photoconductive switches has found particularly widespread use [2, 3]. Terahertz time-domain spectroscopy (THz TDS) [4] has become an established method for phase and amplitude-sensitive measurements with high time resolution and outstanding bandwidth. Recent applications of THz-TDS range from

N. Vieweg (✉) · F. Rettich · A. Deninger
TOPTICA Photonics AG, Lochhamer Schlag 19, 82166 München, Germany
e-mail: nico.vieweg@toptica.com

H. Roehle · R. Dietz · T. Göbel · M. Schell
Fraunhofer Institute for Telecommunications, Heinrich Hertz Institute, Einsteinufer 37, 10587 Berlin, Germany

fundamental research [5, 6], medical diagnostics [7], security applications [8] to non destructive testing [9–12].

THz-TDS instrumentation has come a long way from free-space setups and bulky laboratory equipment to much more compact and inexpensive alternatives. In the past, terahertz pulses were mainly generated with GaAs photoconductive switches, which required laser excitation below 870 nm and often involved complex Ti:Sapphire lasers. With the advent of 1.5 μm fiber lasers and recent InGaAs/InAlAs-based terahertz emitters [13], a trend towards telecom-based technology has become evident. Terahertz spectrometers operating at 1.5 μm take full advantage of mature and cost-efficient telecom components and are thus well suited for real-world applications [14]. These advances notwithstanding, state-of-the-art THz-TDS systems usually achieve the targeted signal-to-noise (SNR) ratios via time-consuming signal averaging methods, which is no hurdle if the quality of the signal is more important than the measurement speed. However, there is still no system on the market that combines fast measurement speed with a top-level SNR performance and high bandwidth. Applications that call for such a system include studies of dynamic processes in biomolecules [15], measurements under rapidly changing environmental conditions, e.g. varying temperatures or magnetic fields [16], and inline process control of plastic materials [17].

In this paper we present a compact fiber-coupled THz-TDS system based on 1.5 μm fiber laser technology and InGaAs/InAlAs photoconductive switches. Due to a precise reconstruction of the time axis, the system drastically reduces the effect of jitter noise and achieves a high dynamic range in conjunction with broad bandwidth and fast measurement speed.

The performance of our system and its key components – femtosecond laser, terahertz antennas and delay stage – are described in the next section of this paper. Special emphasis will then be given to jitter noise and the reconstruction of the time axis. We conclude with application examples in the fields of spectroscopy and imaging.

2 Terahertz time domain spectrometer

2.1 System design and performance

A photograph and a schematic representation of the spectrometer are shown in Figure 1 (a) and (b), respectively. The system comprises a 1.5 μm femtosecond fiber laser with dispersion compensation. A 50 / 50 fiber splitter divides the output beam into an emitter and a detector branch. Both optical paths feature highly precise, fiber-coupled mechanical delay stages: the emitter path includes a fast, scanning delay and the receiver path a slow, long-travel delay. Laser, fiber splitter, delay stages, driver electronics, power supply as well as a microcomputer for system control and data acquisition are all housed in one 19" box (48 x 40 x 20 cm). The system is equipped with an Ethernet data interface to allow flexible control e.g. via LabView software.

The optical pulses in both arms are guided to fiber-coupled, InGaAs-based photoconductive switches, which serve as terahertz emitter and detector. The fiber-pigtailed design permits a flexible arrangement in either transmission or reflection geometry. The emitter converts the laser light into a terahertz pulse [18]. More precisely, the laser pulse excites charge carriers in the emitter antenna, which are accelerated by an externally applied bias field. The resulting current transient gives rise to an electromagnetic pulse - the terahertz pulse that is radiated into free space. The detection process is similar to the generation process. The laser pulse optically

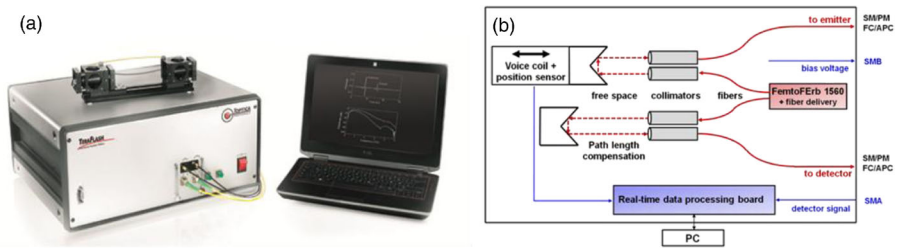


Figure 1 (a) Photograph of the terahertz time-domain system and (b) schematic representation. Blue lines denote electric connections, red lines the optical signal paths.

gates the detector antenna, while the generated charge carriers are accelerated by the electric field of the incident terahertz pulse. The resulting photocurrent is directly proportional to the terahertz electric field. A characteristic of any THz-TDS system is that the width of the generated terahertz pulse (~1 ps) is much longer than the width of the probing laser pulse (~80 fs). Thus, only a fraction of the terahertz pulse is sampled each time the laser pulse hits the detector antenna. To retrieve the full pulse shape, the terahertz pulse is scanned by varying the time delay between the two optical paths.

Figure 2 (a) shows the amplitude spectrum achieved with our system. The terahertz spectrum contains frequency components from 50 GHz to about 4.5 THz with a signal peak at approx. 480 GHz. The inset in Figure 2 (b) presents a typical time-domain signal measured with the system. A single trace of 50 ps can be acquired in only 44 ms. Via the control software, the scan range can be flexibly changed between 15 ps and 200 ps. The width of the terahertz pulse, i.e. the time difference between the maximum and minimum amplitude, amounts to 650 fs.

Figure 2 (b) shows the dependence of the peak dynamic range (PDR) on the number of averaged time traces. For a single measurement (acquisition time 44 ms), the PDR is 60 dB. This value increases with the number of averages: for 100 averages and a total acquisition time of only 4.4 s, a PDR of 82 dB is obtained. The PDR increases to 90 dB for 1000 averages. The

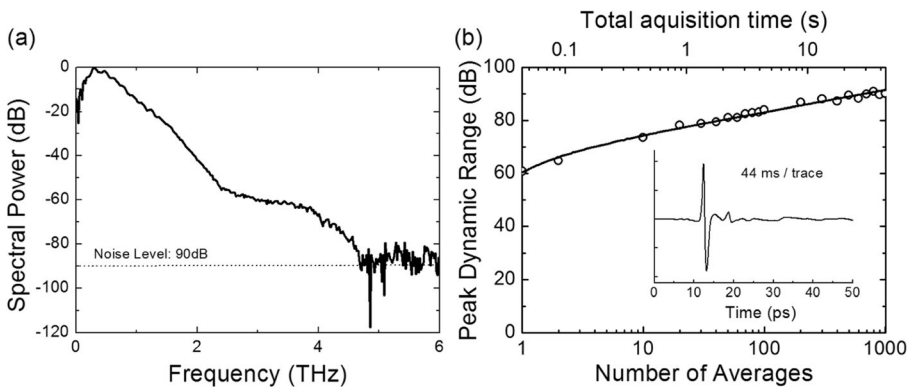


Figure 2 (a) Amplitude spectrum with a bandwidth that exceeds 4.5 THz. (b) Peak dynamic range at 480 GHz versus the number of averaged time traces and total acquisition time. The solid line depicts a fit of Eq. 1. A single trace of 50 ps is measured in 44 ms (inset).

dependence of the peak dynamic range on the number of averages N_{ave} and, consequently, the total measurement time t_{meas} is given by

$$PDR(dB) \propto 20 \log \left(\sqrt{N_{ave}} \right) \propto 20 \log \left(\sqrt{t_{meas}} \right). \quad (1)$$

The PDR of 90 dB presents, to the best of our knowledge, a record for commercial TD-THz systems.

2.2 Femtosecond laser

The spectrometer uses a robust all-fiber-based femtosecond laser system (Toptica FemtoFERb 1560 with fiber delivery FD5-PM). The laser radiation is centered at 1560 nm, the repetition rate is 100 MHz and the pulse width is typically 80 fs. The laser provides approx. 60 mW power at the polarization-maintaining fiber output. Pump diode, active fiber and driver electronics are integrated in one box (21 x 12 x 7.5 cm), which only requires a 12 V external power supply. Both the emitter and the receiver branch employ single-mode, polarization-maintaining fibers of approx. 5 m length. To account for dispersion effects in the fiber delivery, the laser includes dispersion-compensating fibers (DCF) which are spliced into the fiber-optic beam path.

2.3 Delay stages

2.3.1 Long-travel delay line

A long-travel delay line introduces a constant timing offset and thus compensates any changes of the terahertz path and/or fiber length. It comprises a motor-driven corner-cube mirror with a 4-fold optical path, and produces a delay of up to 3000 ps. The value of the time delay is measured with a resolution of 1.3 fs.

2.3.2 Fast and highly precise delay

A second, fast and equally precise delay provides the time variation required for sampling the terahertz pulse with high accuracy. It consists of a voice-coil driven corner-cube mirror combined with a digital, high-precision position sensor. The sensor records 50000 time stamps per second, with a resolution of 1.3 fs. These time stamps are synchronized with the readout of the signal values from the terahertz receiver. Data acquisition is accomplished both during the forward and the backward movement of the mirror, which minimizes the “dead time” of the system. The acquisition time of one pulse trace varies with the chosen delay range, since the swing speed of the voice coil is maintained constant. Consequently, a long travel distance requires more time: The system samples 60 pulses / s for a scan range of 15 ps, whereas a scan range of 200 ps corresponds to 6 pulses / s. The 50 ps traces as shown in Figure 2 (b) are recorded at 22.7 Hz.

The effective scanning speed also depends on the travel distance. The highest rate of 1200 ps / s is attained for the maximum scan range of 200 ps, whilst a 15 ps range is scanned at 900 ps / s. The effective sampling time per step is ~ 25 fs, with even shorter sampling intervals at the turning points of the voice coil. This precise timing resolution gives rise to the high accuracy of the time scale, which results in superior PDR values when multiple traces are averaged.

2.4 Terahertz antennas

The photoconductive emitter employs a high-mobility InAlAs/InGaAs multilayer heterostructure (MLHS) as described in [19, 20]. The receiver is based on an LT-grown Beryllium doped InAlAs/InGaAs MLHS [21, 22] with short carrier lifetime. A strip-line antenna geometry with a 100 μm photoconductive gap was chosen for the emitter, and a dipole geometry with 10 μm gap for the receiver. Both transmitter and receiver feature a mesa-structured gap region as detailed in [13].

The antennas are packaged into compact housings (25 mm diameter) with single-mode, polarization-maintaining fiber pigtailed which guarantee stable optical excitation.

2.5 Impact of jitter on the SNR

In THz-TDS, various noise effects compromise the signal quality [23–25]. Noise contributions include optical and electronic effects [26, 27], laser intensity variations [28], and jitter noise [29, 30]. In the past a lot of effort has been put into reducing electronic detector noise, which played a dominant role in the SNR budget [26, 31]. In this section, we are going to discuss the effect of jitter noise, which has an equally significant impact on the attainable SNR level [25, 29, 32, 33].

Generally, “jitter” denotes a deviation from true periodicity of an assumed periodic signal. In THz-TDS, the terahertz pulse is optically sampled at the detector antenna. More precisely, the terahertz transient is reconstructed from amplitude data acquired in discrete time delay steps. Timing jitter in THz-TDS systems results from a plurality of effects. Whilst contributions that plague free-space laser configurations (e.g., acoustic vibrations of opto-mechanical components, or refractive index fluctuations of air [34]) are largely avoided in our fiber-based design, the timing accuracy of the delay stage itself needs to be taken into account. More specifically, any linear translation stage has a limited length resolution and positional accuracy. Depending on the implementation, the actual position of the delay can differ from the set point by several micrometers [35, 36]. As the optical path length counts two-fold in a delay line with retroreflector, a length difference of only one micrometer already translates into a timing error of 6.6 fs, and the accumulated error can exceed several 10 fs.

Any uncertainty in the time axis leads directly to an uncertainty of the amplitude and thus reduces the dynamic range of the signal. This effect is illustrated in Figure 3. For reasons of clarity a half-wave of a sinusoidal signal $A(t) = \sin(2\pi\nu_{\text{THz}}t)$ with $\nu_{\text{THz}} = 480$ GHz is shown, which corresponds to the PDR frequency of our system. It is evident that a time-domain jitter dt results in an amplitude uncertainty dA . The derivative dA/dt of the sine wave yields

Figure 3 Effect of timing jitter on the signal amplitude.

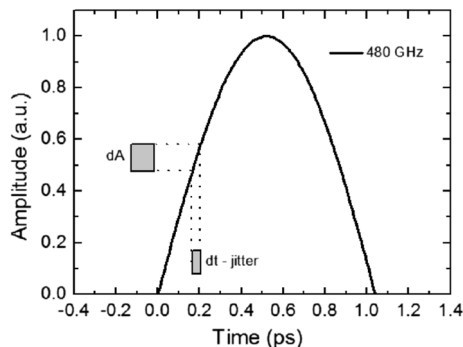
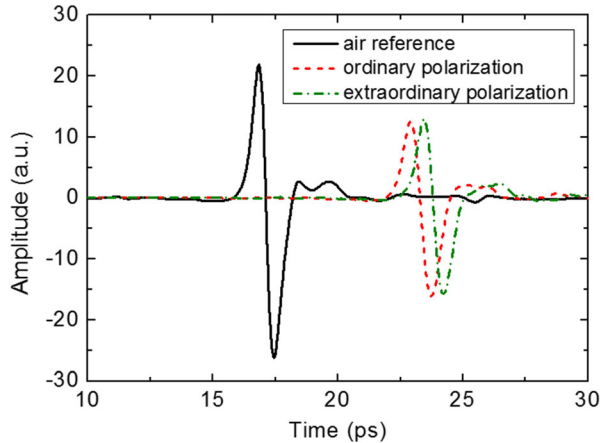


Figure 4 Pulse shift of an anisotropic liquid crystal polymer (LCP) sample.



$2\pi\nu \cos(2\pi\nu t)$. The amplitude uncertainty reaches maximum values at the zero crossings of $A(t)$, i.e. at $t = k / 2\pi\nu$ with $k = 0, 1, 2$, etc. The “worst-case” amplitude error is given by $dA = 2\pi\nu_{THz} dt$ [33] and the dependence of the dynamic range on the timing jitter can be written [37]

$$\text{Dynamic Range}_{\text{jitter}} = -20\log(2\pi\nu_{THz} dt). \quad (2)$$

We note that the absolute value of the PDR depends on a plurality of other factors, such as available terahertz power, the sensitivity of the receiver and electronic noise in the readout circuit. However, Eq. 2 allows us to quantify the influence of the timing jitter in otherwise identical setups.

The system described here determines the delay position with an uncertainty below 400 nm, and thus achieves a time resolution of 1.3 fs. This is an improvement of more than one order of magnitude, compared to the 10 fs level inferred from [35, 36]. Using Eq. 2, we conclude that the precision of the delay stage improves the PDR by more than 17 dB.

3 Application examples

3.1 Terahertz spectroscopy

To demonstrate the suitability of our system for terahertz spectroscopy, we used three different polymer samples: high density polyethylene (HDPE, thickness 1.93 mm), polyamide (PA, 1.07 mm) and E540i,¹ a liquid-crystal polymer (LCP, 2.05 mm). The emitter / receiver modules, optics and the samples themselves were kept in a sealed box, which was purged with dry air to minimize absorption effects by water vapor. Refractive index values and absorption coefficients of the materials were obtained by comparing a reference pulse and a sample pulse, with 1000 averages per trace (measurement time = 44 s). Figure 4 shows a typical trace of a reference pulse in dry air (black solid line), together with pulses which propagated through the LCP sample in ordinary (dashed red line) and extraordinary direction (dashed dotted green line). The orientational order of the LCP molecules gives rise to anisotropic properties: The

¹ E540i is a trademark of TICONA.

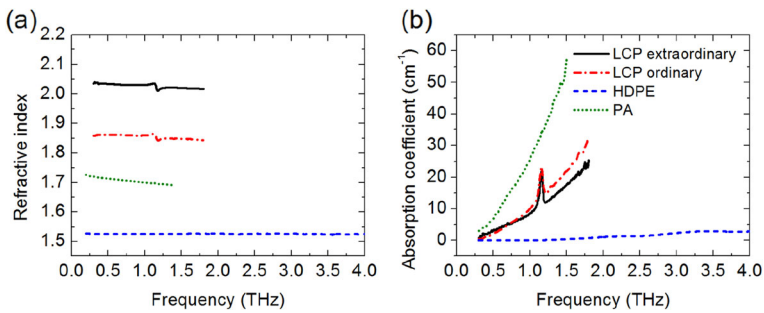


Figure 5 (a) Refractive indices and (b) absorption coefficients of high-density polyethylene (HDPE), polyamide (PA) and a liquid-crystal polymer (LCP) for ordinary and extraordinary polarization.

extraordinary refractive index is higher than the ordinary refractive index [38, 39] and consequently, the pulse undergoes a larger time shift in the case of extraordinary polarization. Note that the pulse amplitudes are nearly identical for both polarizations, indicating similar absorption coefficients.

For extraction of the material parameters we used a quasi-space algorithm [40]. Refractive indices and absorption coefficients are shown in Figure 5 (a) and (b), respectively. The strong absorption of the terahertz wave in the LCP and PA samples at high frequencies lowers the dynamic range and consequently restricts the frequency span useable for analysis to ~ 2 THz.

A nonpolar polymer, HDPE exhibits the lowest absorption (dashed blue line). For this sample almost the full bandwidth of the system is exploited. The absorption coefficient remains < 0.1 cm⁻¹ for frequencies below 1 THz, and increases slightly towards higher frequencies (approx. 1 cm⁻¹ @ 2 THz). The refractive index of 1.53 shows no dispersion over the entire frequency range investigated. In contrast to HDPE, PA is a polar plastic. Our measurements yield a higher, more rapidly increasing absorption coefficient (dotted green line). The refractive index of PA is 1.71 at 0.5 THz and decreases very slightly towards higher frequencies. Our results for PA and HDPE are in very good agreement with literature data [41].

The refractive indices of the LCP show a distinct anisotropy: at 0.5 THz, values for ordinary and extraordinary polarization amount to 1.86 and 2.03, respectively. The dispersive feature at around 1.2 THz corresponds to a distinct absorption peak, as seen in Fig. 5 (b). Note that at higher frequencies, the absorption coefficients follow different trends: The ordinary parameter rises faster than the extraordinary parameter. The absorption peak itself is caused by Talcum, a filling material, which is commonly added to LCP samples [42].

Figure 6 (a) Constituent parts of the birthday card: loudspeaker and circuit board. (b) Photograph and overlay terahertz image of the envelope.

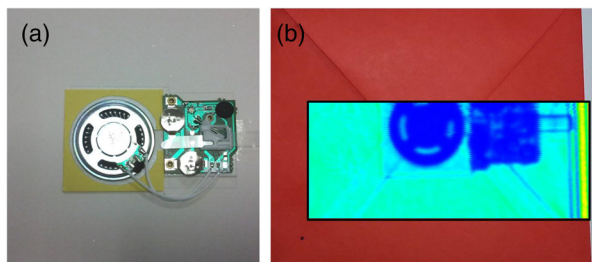
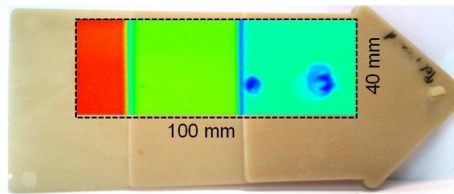


Figure 7 Photograph and overlay terahertz image of a polyamide step wedge.



3.2 Terahertz imaging

Besides terahertz spectroscopy, our system also lends itself for terahertz imaging. For proof-of-principle experiments, two test samples - a mail envelope with an enclosed birthday card featuring a built-in sound chip, and a polyamide step wedge - were mounted on an XY-scanner and moved through the focus of the terahertz beam. Figure 6 shows a photograph of the red envelope that contained the birthday card, and the corresponding terahertz image. The size of the scanned area was 150 mm x 60 mm and the step size was 0.5 mm. The XY-scanner moved at a speed of 3 mm / s, resulting in a total measurement time just below two hours. The terahertz image clearly reveals the electronic board, and the speaker at the center of the envelope.

Figure 7 shows a photograph of the polyamide step wedge and a 100 mm x 40 mm terahertz image. The scan speed was 2 mm / s, the step size was 0.3 mm and the total measurement time was 65 min. Red and blue colors denote sample regions with highest and lowest transmission, respectively, which correspond to the thinnest and thickest sections of the step wedge. The two dark-blue spots reveal air bubbles, which are not visible from the outside. This result demonstrates the suitability of the system for non-destructive testing.

4 Conclusion and Outlook

In conclusion we have designed and characterized a compact, fiber-coupled terahertz time-domain spectrometer operating at an excitation wavelength of 1.5 μm . The system combines mature telecom technology and photoconductive switches based on InAlAs/InGaAs multi-layer heterostructures. Owing to a highly precise mechanical delay stage, the spectrometer offers an outstanding dynamic range, along with a broad bandwidth and high measurement speed. Data acquisition rates range from 6 pulses / s to 60 pulses / s for sampling times of 200 ps and 15 ps, respectively. A precise reconstruction of the time axis reduces the timing jitter to approx. 1.3 fs, which translates into a peak dynamic range of 90 dB and an overall bandwidth of more than 4.5 THz, within a measurement time of less than one minute.

Acknowledgement The authors would like to thank Nicola Kocic of the Süddeutsche Kunststoffzentrum (SKZ) for providing the polyamide sample.

Open Access This article is distributed under the terms of the Creative Commons Attribution License which permits any use, distribution, and reproduction in any medium, provided the original author(s) and the source are credited.

References

1. D. Saeedkia, Ed., *Handbook of terahertz technology for imaging sensing and communications*. Woodhead Publishing Series in Electronic and Optical Materials, 2013.

2. M. van Exter, C. Fattinger, and D. Grischkowsky, "Terahertz time-domain spectroscopy of water vapor," *Opt. Lett.*, vol. 14, pp. 1128–1130, 1989.
3. D. Grischkowsky, S. Keiding, M. van Exter, and C. Fattinger, "Far-infrared time-domain spectroscopy with terahertz beams of dielectrics and semiconductors," *J Opt Soc Am B*, vol. 7, pp. 2006–2015, 1990.
4. P. U. Jepsen, D. G. Cooke, and M. Koch, "Terahertz spectroscopy and imaging – Modern techniques and applications," *Laser Photonics Rev.*, vol. 5, pp. 124–166, 2011.
5. M. Zalkovskij, C. Z. Bisgaard, A. Novitsky, R. Malureanu, D. Savastru, A. Popescu, P. U. Jepsen, and V. Lavrinenko, "Ultrabroadband terahertz spectroscopy of chalcogenide glasses," *Appl. Phys. Lett.*, vol. 100, p. 031901, 2012.
6. S. Tani, F. Blanchard, and K. Tanaka, "Ultrafast carrier dynamics in graphene under high electric field," *Phys. Rev. Lett.*, vol. 109, p. 166603, 2012.
7. C. H. Zhang, G. F. Zhao, B. B. Jin, Y. Y. Hou, H. H. Jia, J. Chen, and P. H. Wu, "Terahertz imaging on subcutaneous tissues and liver inflamed by liver cancer cells," *Terahertz Sci. Technol.*, vol. 5, no. 3, pp. 114–123, 2012.
8. H.-B. Liu, H. Zhong, N. Karpowicz, Y. Chen, and X.-C. Zhang, "Terahertz Spectroscopy and Imaging for Defense and Security Applications," *Proc. IEEE*, vol. 95, no. 8, pp. 1514–1527, Aug. 2007.
9. M. C. Beard, G. M. Turner, and C. A. Schmuttenmaer, "Terahertz spectroscopy," *J. Phys. Chem. B*, vol. 106, pp. 7146–7159, 2002.
10. J. A. Zeitler, P. F. Taday, D. A. Newnham, M. Pepper, K. C. Gordon, and T. Rades, "Terahertz pulsed spectroscopy and imaging in the pharmaceutical setting - A review," *J. Pharm. Pharmacol.*, vol. 59, pp. 209–223, Feb. 2007.
11. C. A. Schmuttenmaer, "Exploring Dynamics in the Far-Infrared with Terahertz Spectroscopy," *Chem. Rev.*, vol. 104, pp. 1759–1779, 2004.
12. D. M. Mittleman, M. Gupta, R. Neelamani, R. G. Baraniuk, J. V. Rudd, and M. Koch, "Recent advances in terahertz imaging," *Appl. Phys. B*, vol. 68, pp. 1085–1094, 1999.
13. H. Roehle, R. J. B. Dietz, H. J. Hensel, J. Böttcher, H. Künzel, D. Stanze, M. Schell, and B. Sartorius, "Next generation 1.5 μm terahertz antennas: mesa-structuring of InGaAs / InAlAs photoconductive layers," *Opt. Express*, vol. 18, pp. 2296–2301, 2010.
14. B. Sartorius, H. Roehle, H. Künzel, J. Böttcher, M. Schlak, D. Stanze, H. Venghaus, and M. Schell, "All-fiber terahertz time-domain spectrometer operating at 1.5 μm telecom wavelengths," *Opt. Express*, vol. 16, no. 13, pp. 9565–9570, 2008.
15. D. M. Leitner, M. Gruebele, and M. Havenith, "Solvation dynamics of biomolecules: modeling and terahertz experiments," *HFSP J*, vol. 2, no. 6, pp. 314–323, Dec. 2008.
16. D. Molter, F. Ellrich, T. Weinland, S. George, M. Goiran, F. Keilmann, and R. Beigang, "High-speed terahertz time-domain spectroscopy of cyclotron resonance in pulsed magnetic field," *Opt. Express*, vol. 18, no. 25, pp. 26163–26168, 2010.
17. N. Krumbholz, T. Hochrein, N. Vieweg, I. Radovanovic, I. Pupeza, M. Schubert, K. Kretschmer, and M. Koch, "Degree of Dispersion of Polymeric Compounds Determined With Terahertz Time-Domain Spectroscopy," *Polym Eng Sci*, vol. 51, pp. 109–116, 2011.
18. D. H. Auston, K. P. Cheung, and P. R. Smith, "Picosecond photoconducting Hertzian dipoles," *Appl. Phys. Lett.*, vol. 45, p. 284, 1984.
19. R. J. B. Dietz, M. Gerhard, D. Stanze, M. Koch, B. Sartorius, and M. Schell, "THz generation at 1.55 μm excitation: six-fold increase in THz conversion efficiency by separated photoconductive and trapping regions," *Opt. Express*, vol. 19, pp. 25911–25917, 2011.
20. R. J. B. Dietz, B. Globisch, M. Gerhard, A. Velauthapillai, D. Stanze, and M. Schell, "64 μW pulsed terahertz emission from growth optimized InGaAs/InAlAs heterostructures with separated photoconductive and trapping regions," *Appl. Phys. Lett.*, vol. 103, no. 6, p. 061103, 2013.
21. B. Globisch, R. J. B. Dietz, D. Stanze, T. Göbel, and M. Schell, "Carrier dynamics in Beryllium doped low-temperature-grown InGaAs/InAlAs," *Appl. Phys. Lett.*, vol. 104, p. 172103, Apr. 2014.
22. R. J. B. Dietz, B. Globisch, H. Roehle, D. Stanze, T. Göbel, and M. Schell, "Influence and adjustment of carrier lifetimes in photoconductive pulsed terahertz detectors based on InGaAs/InAlAs: Towards 6 THz bandwidth and 90 dB dynamic range," *Submit. to Opt. Express*.
23. P. U. Jepsen and B. M. Fischer, "Dynamic range in terahertz time-domain transmission and reflection spectroscopy," *Opt Lett*, vol. 30, no. 1, pp. 29–31, Jan. 2005.
24. W. Withayachumnankul, B. M. Fischer, H. Lin, and D. Abbott, "Uncertainty in terahertz time-domain spectroscopy measurements," *J Opt Soc Am B*, vol. 25, pp. 1059–1072, 2008.
25. W. Withayachumnankul, H. Lin, S. P. Mickan, B. M. Fischer, and D. Abbott, "Analysis of Measurement Uncertainty in THz-TDS," *Proc SPIE*, vol. 6593, pp. 659326–659326–18, May 2007.
26. M. van Exter and D. Grischkowsky, "Characterization of an optoelectronic terahertz beam system," *IEEE Trans. Microw. Theory Tech.*, vol. 38, pp. 1684–1691, 1990.

27. L. DuVillaret, F. Garet, and J.-L. Coutaz, “Influence of noise on the characterization of materials by terahertz time-domain spectroscopy,” *J Opt Soc Am B*, vol. 17, pp. 452–460, 2000.
28. H. A. Haus and A. Mecozzi, “Noise of mode-locked lasers,” *IEEE J. Quantum Elect.*, vol. 29, pp. 983–996, 1993.
29. A. Wojdyła and G. Gallot, “Phase noise investigation in terahertz Time-Domain Spectroscopy measurements,” *Proc IRMMW*, 2013.
30. N. Cohen, J. W. Handley, R. D. Boyle, S. L. Braunstein, and E. Berry, “Experimental Signature of Registration Noise in Pulsed Terahertz Systems,” *Fluct Noise Lett*, vol. 6, no. 0, pp. L77–L84, 2006.
31. E. Castro-Camus, L. Fu, J. Lloyd-Hughes, H. H. Tan, C. Jagadish, and M. B. Johnston, “Photoconductive response correction for detectors of terahertz radiation,” *J. Appl. Phys.*, vol. 104, no. 5, p. 053113, 2008.
32. X. Xu, X. Wang, and L. Wang, “Deviation of optical constants extracted in terahertz transmission spectroscopy,” *Appl. Opt.*, vol. 45, no. 4, pp. 648–52, Feb. 2006.
33. J. Letosa, M. García-Gracia, J. M. Forniés-Marquina, and J. M. Artacho, “Performance Limits in TDR Technique by Monte Carlo Simulation,” *IEEE T Magn*, vol. 32, pp. 4–7, 1996.
34. S. M. Rytov, Y. A. Kravtsov, and V. I. Tatarskii, *Principles of statistical radiophysics 4. Wave propagation through random media*. Springer Verlag, 1989.
35. M. Theuer, R. Beigang, and D. Grischkowsky, “Highly sensitive terahertz measurement of layer thickness using a two-cylinder waveguide sensor,” *Appl. Phys. Lett.*, vol. 97, no. 7, p. 071106, 2010.
36. C. D. Stoik, “Nondestructive evaluation of aircraft composites using terahertz time domain spectroscopy,” *PhD Thesis, Air Force Inst. Technol.*, 2008.
37. L. Wu, “Optimierung des Signal-Rausch-Abstands von AD-Wandlern,” *Elektron. Ind.*, vol. 11, pp. 50–52, 2010.
38. N. Vieweg, B. M. Fischer, M. Reuter, P. Kula, R. Dabrowski, M. a. Celik, G. Frenking, M. Koch, and P. U. Jepsen, “Ultrabroadband terahertz spectroscopy of a liquid crystal,” *Opt. Express*, vol. 20, no. 27, pp. 28249–28256, Dec. 2012.
39. N. Vieweg and A. Deninger, “Terahertz waves and liquid crystals: prospects and challenges,” *Proc. SPIE*, vol. 8642, p. 86420, 2013.
40. M. Scheller, C. Jansen, and M. Koch, “Analyzing sub-100- μm samples with transmission terahertz time domain spectroscopy,” *Opt. Commun.*, vol. 282, pp. 1304–1306, 2009.
41. R. Piesiewicz, C. Jansen, S. Wietzke, D. Mittleman, M. Koch, and T. Kürner, “Properties of Building and Plastic Materials in the THz Range,” *Int J Infrared Milli Terahz Waves*, vol. 28, pp. 363–371, 2007.
42. U. A. Khan, N. Nguyen, and M. N. Afsar, “Millimeter and submillimeter-wave dielectric measurements of household powders using fourier transform spectroscopy,” *IEEE T Instrum Meas*, vol. 57, no. 2, pp. 286 – 293, 2008.